Fiber Bragg Grating Sensor Simulation for Corona Discharge Temperature Sensor

Aulia Izzuddin Laksono
Department of Electrical Engineering, Faculty of Engineering, Universitas Indonesia Kampus Baru UI Depok

Fauzan Hanif Jufri
Department of Electrical Engineering, Faculty of Engineering, Universitas Indonesia Kampus Baru UI Depok

Apriono, Catur
Department of Electrical Engineering, Faculty of Engineering, Universitas Indonesia Kampus Baru UI Depok

https://doi.org/10.5109/4794179

出版情報：Evergreen. 9 (2), pp.506-510, 2022-06. 九州大学グリーンテクノロジー研究教育センター
バージョン：

Fiber Bragg Grating Sensor Simulation for Corona Discharge Temperature Sensor

Aulia Izzuddin Laksono[1], Fauzan Hanif Jufri[1], Catur Apriono[1,*]
[1]Department of Electrical Engineering, Faculty of Engineering, Universitas Indonesia
Kampus Baru UI Depok, Jawa Barat, Indonesia

*Author to whom correspondence should be addressed:
E-mail: catur@eng.ui.ac.id

(Received February 11, 2022; Revised June 20, 2022; accepted June 20, 2022).

Abstract: Corona discharge causes a change in temperature on a material surface because of the change in heat coefficient. Visual inspection is the common technique for corona discharge inspection, which costs time and energy. Therefore, developing a remote sensing system is necessary to monitor the phenomenon. This study considers fiber Bragg grating as an optical sensor to sense temperature changes using OptiSystem simulation software. The response spectrum of the reflected signal changes its center wavelength as the simulated temperature changes produce a linear equation of 0.014294 times its temperature change for the initial model, and temperature changes decreasingly by considering heat transfer experiment data. The proposed results show its prospective for further development and implementation.

Keywords: fiber Bragg grating, temperature, sensor, corona discharge, heat transfer

1. Introduction

Corona discharge has been one of the major problems in high voltage transmission lines. It may cause a problem for the intended uninterrupted energy supply, which is essential for sustainable economic growth[1)2)3)]. The common detection method relies on visual inspection by eye or ultraviolet thermal camera[4)]. Those techniques consume a lot of time and need solutions to detect and monitor effectively and efficiently.

A sensor is needed to sense corona's physical quantities and then convert it into electrical signals[5)]. One sensor based on the optical principle that has found itself in a wide range of applications is fiber Bragg grating (FBG), which in particular has been used in rotor hotspot detection[6)], structural health monitoring (SHM)[7)], and transformer oil degradation[8)]. It has two main sensing abilities, which are temperature and strain sensing. Both can be modified into sensing other things like water pollution levels, humidity, ultraviolet radiation, and more. On the other hand, optical ground wire (OPGW) is an integral part of any power company's transmission network used for grounding and data transmission through fiber optic. Hence, FBG can be implemented by utilizing the OPGW to monitor the possibility of corona occurrence in the transmission line.

Corona discharge causes heat transfer enhancement, providing a temperature change on the surface of the electrodes or conductors[9)]. This study performs a simulation to detect the temperature change on the surface of the electrodes or conductors by using an FBG. The simulation is carried out using OptiSystem and varying the temperature. The concept of the FBG is explained in Section II, the simulation setup and the parameters used in the simulation are provided in Section III, the results are presented in Section IV, and lastly, Section V concludes this research. Researchers or transmission line engineers may use the methodology explained to conduct more advanced research on FBG sensors.

2. Fiber Bragg Grating

2.1 Basic Principle

According to IEEE Std 2067-2021, FBG is a phase diffraction grating integrated with optical single-mode silica fiber to selectively reflect a very narrow range of wavelengths while transmitting others. To achieve that characteristic, periodically spaced zones in the fiber optic core need slightly higher refractive indexes than the core. Equations 1 and 2 indicate that the difference between refractive indexes causes path and phase differences. $\Delta\Gamma$ and $\Delta\phi$ is path difference and phase difference respectively, Λ is the distance between grating, θ is the angle measured from the normal boundary in the grating, and n is the grating's refractive index.

$$\Delta\Gamma = (2\Lambda \tan\theta)(\sin\theta') = 2n\Lambda\cos\theta \quad (1)$$

$$\Delta\phi = 2\pi\frac{2n\Lambda}{\lambda}\cos\theta \quad (2)$$

Reflected light from the grating's surface and bottom interfere with each other. In FBG, constructive interference is desired; therefore, phase shift needs to happen in multiples of 2π. So, suppose we substitute the $2\pi/\lambda$ with wavenumber and θ = 0 because fiber-optic light comes perpendicular to the grating's surface. In that case, the variables affecting the characteristic of the reflected light of FBG can be simplified into $2n\Lambda$, representing its center wavelength (λ_B) as shown in Equation 3[10]. n_{eff} is the average refractive index of the gratings. In principle, FBG will receive a light signal, then reflect a signal with λB as center wavelength, and let other wavelengths through or transmitted.

$$\lambda_B = 2n_{eff}\Lambda \tag{3}$$

2.2 Temperature Effect on FBG

Fiber Bragg grating can be used as sensors because their signal parameters change when certain physical changes occur. Some of the physical parameters that can be measured changes include temperature, mechanical strain, humidity, chemical concentration, light intensity, refractive index, etc[16)17)21)]. The parameter list will continue to grow as research utilizes Bragg lattice fibers. Equation 4 shows the physical changes based on Bragg wavelength shift ($\Delta\lambda_B$). L represents the strain, the wavelength, and T represents the temperature. In addition, Equation 5 is an equation based on the thermal coefficient that can be used to determine the change in the refractive index. ζ represents the thermo-optic coefficient and the change in the grating period. η represents the thermo-optic expansion coefficient[10)].

$$\Delta\lambda_B = 2\left(\Lambda\frac{\delta n_{eff}}{\delta L} + n_{eff}\frac{\delta\Lambda}{\delta L}\right)\Delta L + 2\left(\Lambda\frac{\delta n_{eff}}{\delta\lambda} + n_{eff}\frac{\delta\Lambda}{\delta\lambda}\right)\Delta\lambda + 2\left(\Lambda\frac{\delta n_{eff}}{\delta T} + n_{eff}\frac{\delta\Lambda}{\delta T}\right)\Delta T \tag{4}$$

$$\Delta n = \zeta n \Delta T \tag{5}$$

$$\Delta n = \eta\Lambda(T - T_{ref}) \tag{6}$$

3. Simulation Setup

This study considers OptiSystem to simulate an FBG sensor and the temperature changes from a determined model. Another consideration is the heat transfer experiment from the other research to represent the corona discharge data experiment[9)]. The last data is considered the basis for the corona discharge phenomenon.

Figure 1 shows a schematic of the FBG sensor setup. One considered FBG is under one measurement point. An optical source with a 1550 nm center wavelength with -20 dBm spectral density is paired with an optical circulator to direct the light to the sensor. The reflected light is directed to Optical Spectrum Analyzer (OSA) via a circulator. Optical Power Meter is necessary to check the power level in each component.

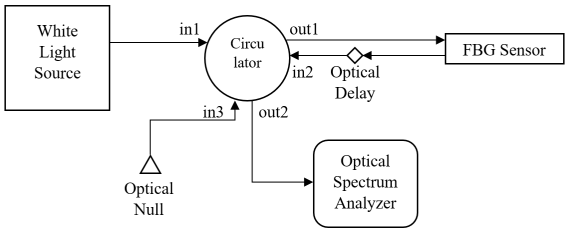

Fig. 1: Schematic of FBG sensor setup

3.1 Simulation Parameter

Modulation Index and Modal Index: The modulation index value (Δ_{no}) represents the change in the modulation index due to the fabrication of Bragg lattice fibers. The determined modulation index value is 0.0005 so that the index change (Δ) is much smaller relative to the optical fiber refractive index (n_o) ($\Delta << n_o$). These requirements ensure that the average modulation index of the Bragg lattice fiber is uniform. However, the refractive index value also affects the change in the average refractive index. It is because of the shape of the lattice fiber, the chirp function, and the apodization function[10)]. The smaller the value of the modulation index, chirp, apodization, and others, the weaker the effect will change the average refractive index. The modal index represents the refractive index of the fiber optic core. Typical values are in the range of 1.44 to 1.46.

1) Overlap Integral: The overlap integral value is the confinement factor of the optical fiber used. In the simulation, the default value of the simulator is 0.8, which states that 80% of the energy confined to the optical fiber core is relative to the total energy.

2) Apodization Functions and Parameter: The index change factor is important to get the desired reflected signal result. In the simulator, apodization can only be selected without apodization or Gaussian apodization. Gaussian apodization clarifies the difference between the center of the reflected signal wave to be read and the side lobe. Gaussian apodization in the physical Bragg lattice fibers seems to darken the top and bottom edges of the grating to produce a suppressed side lobe. Changes in the side lobes occur due to changes in the aperture in the fiber. In the simulation, the value of the G parameter is also still using the simulator default value of 0.5. If fabrication is carried out, the value of parameter *G* can be adjusted again according to the specifications of the fabricator's tools and techniques.

3) Grating Length: Grating length represents the distance between the first and last grating in fiber or the length of the measuring point. This study considers a value of 7 mm. It was neither too long nor too short relative to the aluminum's length and width in the literature's corona discharge test (70 mm × 50 mm)[9].

4) Strain Sensor Parameters: The simulator can also simulate the strain felt by the sensor. The Poisson ratio values represent the mechanical parameters of the lattice fibers for the longitudinal strain. In contrast, the P11 and P12 values represent the photo-elastic coefficients for the strains in the defined planes P11 and P12.

5) Temperature Sensor Parameter: The thermo-optical coefficient represents the change in refractive index due to temperature. The thermal expansion coefficient represents the shift in the center of the wavelength due to temperature. Changes in the actual index of refraction will also affect the center wavelength of the Bragg lattice fiber. The value of the thermo-optical coefficient and the coefficient of thermal expansion are $8.3 \times 10^{-6}/℃$ and $5.5 \times 10^{-7}/℃$, respectively, were obtained based on literature[11].

6) Simulation Parameters: The parameters for simulating temperature changes are based on the reference temperature for the values of the parameters that have been previously set, and then the readings are set for each temperature iteration. The temperature function can be linear or follow certain equations. In the simulation, the reference temperature is set at 0℃ to make it easier to read the graph so that the resulting graph is a shift in wavelength based on temperature changes.

7) Optical Circulator Parameters: Generally, the optical circulator parameter values are designed to have a low insertion loss and high isolation and return loss. The low insertion loss ensures that the signal entering the circulator does not suffer as much loss as the optical fiber is connected to the circulator port. The isolation value is designed high so that the signal does not return to its input port. For example, the signal enters the input port one to not return to the output port 3. At the same time, the return loss value is selected high so that the signal is transmitted properly and inconsiderable is reflected. The selection of insertion loss values of 0.5 dB, return loss of 50 dB, and isolation of 45 dB in the simulation is based on the values listed on optical circulators circulating in online stores. This condition is expected to minimize the difference in reading values when the experiment is carried out.

3.2 Auxiliary Simulation Components

As noticed in Figure 1, there are two components with no parameter but are important in simulating the circuit: optical delay and optical null. Both must be present so the interrogator can read the reflected light. Before simulating, it must be set that the iteration count is more than one. Optical delay causes the reflected signal to be calculated in the second iteration. This condition is essential because OptiSystem treats reflected and transmitted signals into a different calculation iteration. So, for an interrogator to read the signal reflected by FBG, the signal must be delayed, and the signal index in OSA changed to 1 from default value 0. Optical null also causes the circulator to multiplex the port3 input with null signal, so no signal is coming out from port1 output. Additionally, when simulating the temperature, the sweep feature is recommended so that the simulated temperature does not have to be input manually for every simulation.

4. Simulation Result

The simulation results were obtained by the optical spectrum analyzer as shown in Figure 2 at the reference temperature (0°C). The reflected signal has a center wavelength of 1550 nm according to the FBG parameter setting. The signal has a power of 70 dBm, with the sidelobe having a power difference above -20 dBm.

Figure 3 shows the simulation results of the center wavelength versus temperature. The linear equation is 0.014294 * T + 1550 nm. It means, every one degree of temperature increase will cause the center of the reflected wavelength to change by 0.014294 nm.

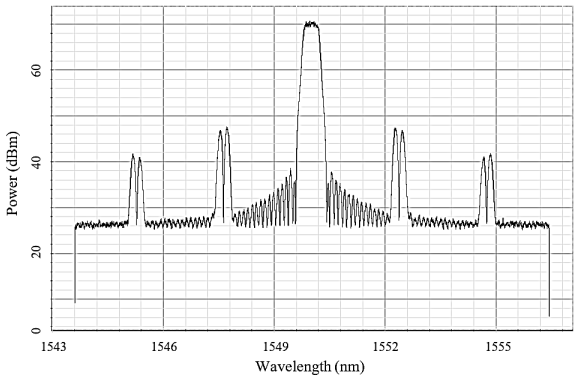

Fig. 2: Reflected signal at reference temperature (0°C).

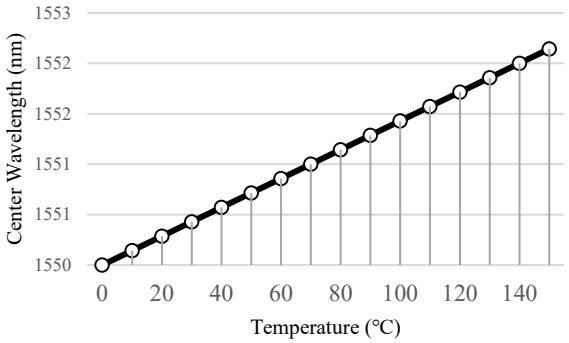

Fig. 3: Center wavelength versus temperature

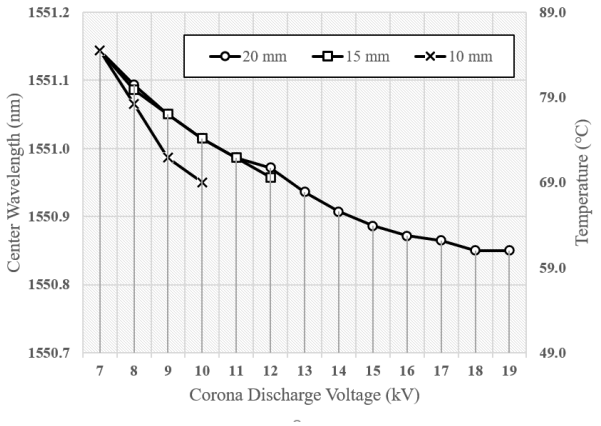

Fig. 4: Predicted wavelength and temperature versus corona discharge voltage

After considering OptiSystem to simulate an FBG sensor and the temperature changes from a determined model, another consideration is the heat transfer experiment from the other research to represent the corona discharge data from the experiment[9]. Figure 4 shows the center wavelength when the temperature sensor calibration results are at 1550 nm at a temperature of 0℃, and the thermo-optical coefficient value is 8.3 × 10-6/℃. The thermal expansion coefficient is 5.5 × 10-7/℃. Sensors with different wavelength centers will produce different spectrum and center wavelength readings on an optical spectrum analyzer.

5. Conclusion

A temperature sensor model has been designed using Bragg lattice fibers. The response spectrum of the reflected signal changes its center wavelength as the simulated temperature changes produce a linear equation of 0.014294 * T for the initial model and temperature changes decreasingly by considering heat transfer experiment data. The proposed results show its prospective for further development and implementation. Future work expects that the temperature sensing by FBG through the OPGW can be extended to distinguish the corona discharge in the transmission line.

Acknowledgments

Ministry of Research and Technology / National Agency for Research and Innovation, Republic of Indonesia supports this research through Penelitian Dasar Grant, contract number: NKB-028/UN2.RST/HKP.05.00/2021, the year 2021.

References

1) M.K. Barai, and B.B. Saha, “Energy Security and Sustainability in Japan,” *Evergr. Jt. J. Nov. Carbon Resour. Sci. Green Asia Strateg.*, **02** (*01*) 49–56 (2015).
2) M. Bansal, A. Agarwal, M. Pant, and H. Kumar, “Challenges and Opportunities in Energy Transformation During Covid-19,” *Evergr. Jt. J. Nov. Carbon Resour. Sci. Green Asia Strateg.*, **8** (*2*) 255–261 (2021). doi:10.5109/4480701.
3) R. Yoneda, “Research and technical trend in nuclear fusion in japan,” *Evergreen*, **04** (*4*) 16–23 (2017). doi:10.5109/1929677.
4) Y. Kim, and K. Shong, “The Characteristics of UV Strength According to Corona Discharge From Polymer Insulators Using A UV Sensor and Optic Lens,” *IEEE Trans. Power Deliv.*, **26** (*3*) 1579–1584 (2011). doi:10.1109/TPWRD.2011.2131689.
5) H. Prasetyo, “On-grid photovoltaic system power monitoring based on open source and low-cost internet of things platform,” *Evergr. Jt. J. Nov. Carbon Resour. Sci. Green Asia Strateg.*, **08** 98–106 (2021). doi:10.5109/4372265.
6) C. Hudon, M. Lévesque, M. Essalihi, and C. Millet, “Investigation of rotor hotspot temperature using Fiber Bragg Gratings,” in: 2017 IEEE Electr. Insul. Conf. EIC 2017, Institute of Electrical and Electronics Engineers Inc., 2017: pp. 313–316. doi:10.1109/EIC.2017.8004671.
7) D. Kinet, P. Mégret, K.W. Goossen, L. Qiu, D. Heider, and C. Caucheteur, “Fiber bragg grating sensors toward structural health monitoring in composite materials: challenges and solutions,” *Sensors (Switzerland)*, **14** (*4*) 7394–7419 (2014). doi:10.3390/S140407394.
8) B.I. Onn, P.T. Arasu, Y. Al-Qazwini, A.F. Abas, N. Tamchek, and A.S.M. Noor, “Fiber bragg grating sensor for detecting ageing transformer oil,” *ICP 2012 - 3rd Int. Conf. Photonics 2012, Proc.*, 110–113 (2012). doi:10.1109/ICP.2012.6379520.
9) Y.Y. Tsui, Y.X. Huang, C.C. Lan, and C.C. Wang, “A study of heat transfer enhancement via corona discharge by using a plate corona electrode,” *J. Electrostat.*, **87** 1–10 (2017). doi:10.1016/J.ELSTAT.2017.02.003.
10) R. Kashyap, “Fiber Bragg Gratings,” Elsevier Inc., 2010. doi:10.1016/C2009-0-16830-7.
11) S. Kanakambaran, R. Sarathi, and B. Srinivasan, “Robust classification of partial discharges in transformer insulation based on acoustic emissions detected using fiber bragg gratings,” *IEEE Sens. J.*, **18** (*24*) 10018–10027 (2018). doi:10.1109/JSEN.2018.2872826.
12) H.Nurjannah, F.A.Z.M. Saat, F.S. Anuar, and D. Johari, “Temperature and velocity changes across tube banks in one-directional and bi-directional flow conditions hasbullah, nurjannah temperature and velocity changes across tube banks in one-directional and bi-directional flow conditions,” *Evergr. Jt. J. Nov. Carbon Resour. Sci. Green Asia Strateg.*, **08** (*02*)

428–437 (2021). doi:10.5109/4480725.
13) S. Choudhary, A. Sharma, K. Srivastava, H. Purohit, and M. Vats, "Read Range Optimization of Low Frequency RFID System in Hostile Environmental Conditions by Using RSM Approach," *Evergr. Jt. J. Nov. Carbon Resour. Sci. Green Asia Strateg.*, **07** (*3*) 396–403 (2020).
14) S. Kanakambaran, R. Sarathi, and B. Srinivasan, "Robust classification of partial discharges in transformer insulation based on acoustic emissions detected using fiber bragg gratings," *IEEE Sens. J.*, **18** (*24*) 10018–10027 (2018). doi:10.1109/JSEN.2018.2872826.
15) N.A. Rosman, C.B.M. Rashidi, S.A. Aljunid, and R. Endut, "Temperature monitoring system using fiber bragg grating (fbg) approach," *AIP Conf. Proc.*, 985 383 (2020). doi:10.1063/1.5142157.
16) Z. Wang, H. Li, L. Zhang, and J. Xue, "Strain transfer characteristic of a fiber bragg grating sensor bonded to the surface of carbon fiber reinforced polymer laminates," *Appl. Sci. 2018*, Vol. 8, Page 1171, 8 (7) 1171 (2018). doi:10.3390/APP8071171.
17) M. Liang, and X. Fang, "Application of fiber bragg grating sensing technology for bolt force status monitoring in roadways," *Appl. Sci. 2018*, Vol. 8, Page 107, 8 (1) 107 (2018). doi:10.3390/APP8010107.
18) W. Zhang, L. Zhu, M. Dong, X. Lou, and F. Liu, "A temperature fiber sensor based on tapered fiber bragg grating fabricated by femtosecond laser," *Appl. Sci. 2018, Vol. 8*, Page 2616, 8 (12) 2616 (2018). doi:10.3390/APP8122616.
19) Z. Guo, Q. Ye, F. Li, and Y. Wang, "Study on corona discharge spatial structure and stages division based on visible digital image colorimetry information," I*EEE Trans. Dielectr. Electr. Insul.*, 26 (5) 1448–1455 (2019). doi:10.1109/TDEI.2019.008054.
20) M. Liu, J. Tang, Q. Yao, and Y. Miao, "Development processes of positive and negative dc corona under needle-plate electrode in air," *ICHVE 2016 - 2016 IEEE Int. Conf. High Volt. Eng. Appl.*, (2016). doi:10.1109/ICHVE.2016.7800827.
21) S.C. Her, and W.N. Lin, "Simultaneous measurement of temperature and mechanical strain using a fiber bragg grating sensor," *Sensors (Switzerland)*, 20 (15) 1–12 (2020). doi:10.3390/S20154223.
22) G. Callender, and P.L. Lewin, "Modeling partial discharge phenomena," *IEEE Electr. Insul. Mag.*, 36 (2) 29–36 (2020). doi:10.1109/MEI.2020.9070114.
23) R.P. Nair, and S.B. Vishwanath, "A novel approach to identify slot discharges in the presence of end winding corona discharges," *IEEE Trans. Dielectr. Electr. Insul.*, 26 (5) 1385–1393 (2019). doi:10.1109/TDEI.2019.007959.
24) F. Yin, M. Farzaneh, and X. Jiang, "Laboratory investigation of ac corona loss and corona onset voltage on a conductor under icing conditions," *IEEE Trans. Dielectr. Electr. Insul.*, 23 (3) 1862–1871 (2016). doi:10.1109/TDEI.2016.005626.
25) B. He, H. Zhao, C. Chen, S. Liu, and Z. Peng, "Influence of wind speed and dust particle size on the corona characteristics of ± 1100 kv fitting models," *IEEE Trans. Dielectr. Electr. Insul.*, 24 (4) 2432–2439 (2017). doi:10.1109/TDEI.2017.006594.
26) A.M. Abobaker, "TESTING a real time monitoring system for passive optical networks using an array of fiber bragg gratings," *Int. J. New Comput. Archit. Their Appl.*, 4 (4) 146–155 (2014). doi:10.17781/P0014.